ACCOUNTS of chemical research

pubs.acs.org/accounts Article

Ab Initio Direct Dynamics

Published as part of the Accounts of Chemical Research special issue "Direct Dynamics of Chemical Processes and Pathways".

H. Bernhard Schlegel*

Cite This: https://doi.org/10.1021/acs.accounts.1c00390 Read Online

CONSPECTUS: The reactivity and dynamics of molecular systems can be explored computationally by classical trajectory calculations. The traditional approach involves fitting a functional form of a potential energy surface (PES) to the energies from a large number of electronic structure calculations and then integrating numerous trajectories on this fitted PES to model the molecular dynamics. The ever-decreasing cost of computing and continuing advances in computational chemistry software have made it possible to use electronic structure calculations directly in molecular dynamics simulations without first having to construct a fitted PES. In this "on-the-fly" approach, every time the energy and its derivatives are needed for the integration of the equations of motion, they are obtained directly from quantum chemical calculations. This approach started to become practical in the mid-1990s as a result of increased availability of inexpensive computer resources and improved computational chemistry software. The application of direct dynamics calculations has grown rapidly over the last 25 years and would require a lengthy review article. The present Account is limited to some of our contributions to methods development and various applications. To improve the efficiency of direct dynamics calculations, we developed a Hessian-based predictor-corrector algorithm for integrating classical trajectories. Hessian updating made this even more efficient. This approach was also used to improve algorithms for following the steepest descent reaction paths. For larger molecular systems, we developed an extended Lagrangian approach in which the electronic structure is propagated along with the molecular structure. Strong field chemistry is a rapidly growing area, and to improve the accuracy of molecular dynamics in intense laser fields, we included the time-varying electric field in a novel predictor-corrector trajectory integration algorithm. Since intense laser fields can excite and ionize molecules, we extended our studies to include electron dynamics. Specifically, we developed code for time-dependent configuration interaction electron dynamics to simulate strong field ionization by intense laser pulses. Our initial application of ab initio direct dynamics in 1994 was to $CH_2O \rightarrow H_2 + CO$; the calculated vibrational distributions in the products were in very good agreement with experiment. In the intervening years, we have used direct dynamics to explore energy partitioning in various dissociation reactions, unimolecular dissociations yielding three fragments, reactions with branching after the transition state, nonstatistical dynamics of chemically activated molecules, dynamics of molecular fragmentation by intense infrared laser pulses, selective activation of specific dissociation channels by aligned intense infrared laser fields, angular dependence of strong field ionization, and simulation of sequential double ionization.

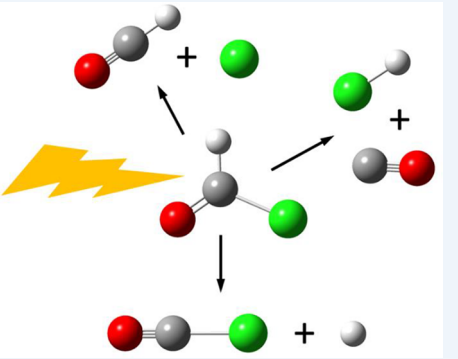

KEY REFERENCES

- Bakken, V.; Millam, J. M.; Schlegel, H. B. Ab initio classical trajectories on the Born-Oppenheimer surface: Updating methods for Hessian-based integrators *J. Chem. Phys.* **1999**, *111*, 8773−8777.[1] *The Hessian-based predictor-corrector algorithm along with Hessian updating methods provides a practical and efficient method for integrating molecular dynamics trajectories "on-the-fly".*
- Schlegel, H. B.; Millam, J. M.; Iyengar, S. S.; Voth, G. A.; Daniels, A. D.; Scuseria, G. E.; Frisch, M. J. Ab initio molecular dynamics: Propagating the density matrix with Gaussian orbitals. *J. Chem. Phys.* **2001**, *114*, 9758−9763.[2] *Atom-centered density matrix propagation (ADMP) is our extended Lagrangian approach in which the electronic structure is propagated along with the molecular structure.*
- Lee, S. K.; Suits, A. G.; Schlegel, H. B.; Li, W. A reaction accelerator: Mid-infrared strong field dissociation yields mode-selective chemistry. *J. Phys. Chem. Lett.* **2012**, *3*, 2541−2547.[3] *The rate for higher energy dissociation*

Received: June 29, 2021

https://doi.org/10.1021/acs.accounts.1c00390
Acc. Chem. Res. XXXX, XXX, XXX−XXX

channels can be selectively enhanced with intense, ultrashort mid-infrared laser pulses if the molecule can be oriented.

- Krause, P.; Schlegel, H. B. Angle-dependent ionization of small molecules by time-dependent configuration interaction and an absorbing potential. *J. Phys. Chem. Lett.* **2015**, *6*, 2140−2146.[4] *For intense, ultrashort laser pulses, the ionization yield has a very strong dependence on the angle between the molecule and the polarization direction of the pulse.*

INTRODUCTION

Classical trajectory calculations can provide detailed information about molecular reactivity and dynamics.[5,6] Conventionally, a potential energy surface is constructed by fitting a functional form to a large number of energies (and possibly gradients) obtained from electronic structure calculations. Trajectories are then integrated using this potential energy function.[7,8] Alternatively, the potential energy surface (PES) needed for the trajectories can be computed "on-the-fly"; every time the energy and its derivatives are needed for integrating the equations of motion, they are obtained directly from quantum chemical calculations. While there were a few early studies,[9,10] direct molecular dynamics with ab initio molecular orbital calculations became practical for small molecules starting in the early 1990s.[11−13] My group became interested in ab initio molecular dynamics (AIMD) through a collaboration with Bill Hase on the $CH_2O \rightarrow H_2 + CO$ dissociation reaction.[13] This early study combined Hase's expertise in molecular dynamics with our background in developing derivative methods for electronic structure calculations[14,15] and algorithms for geometry optimization and reaction path following.[16] This short Account cannot review all of the developments and applications of direct dynamics that have occurred in the last 25 years. Instead, the present discussion is limited to some of our contributions, starting with the early development of methods for ab initio direct molecular dynamics and applications to unimolecular dissociation reactions. These studies and collaborations with Bob Levis and Wen Li led to our interest in the dynamics of molecules in intense laser fields. In turn, this stimulated our studies of electron dynamics and ionization of molecules by ultrashort, intense laser pulses.

METHOD DEVELOPMENT FOR DYNAMICS

Hessian-Based Predictor-Corrector Algorithm

Numerous methods are available for integrating classical equations of motion for molecules on ground state potential energy surfaces. These standard algorithms require only first derivatives of the energy with respect to the atomic coordinates, i.e., the forces or gradients of the PES. Most electronic structure software packages can calculate analytic gradients for several different levels of theory. The problem is that very many small steps are needed to integrate of the trajectories with sufficient accuracy and conservation of energy. Thus, many electronic structure calculations are required, making this approach too costly for widespread application in the 1970s and 1980s. In the early 1990, Helgaker and Uggerud[11,12] demonstrated that much larger steps could be taken if second derivatives or Hessians are used to provide a local quadratic approximation to the PES. By that time a number of codes could calculate analytic second derivatives for Hartree−Fock (HF), density functional theory (DFT), and multiconfiguration SCF (MCSCF). Nevertheless, the method still required many electronic structure calculations for each trajectory. For standard methods using only gradients, predictor-corrector methods improve the accuracy and efficiency. This prompted us to develop a Hessian-based predictor-corrector algorithm for integrating classical trajectories, Figure 1.[13,17]

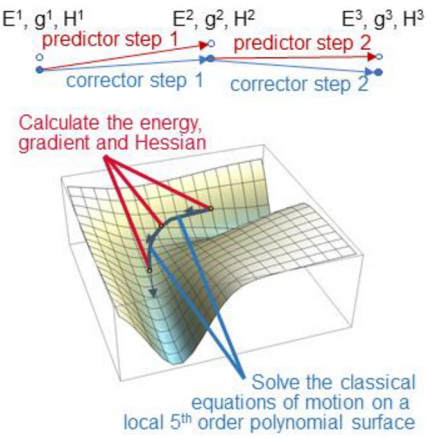

Figure 1. Hessian-based predictor-corrector algorithm for integrating classical trajectories. (Adapted with permission from ref 17. Copyright 1999 AIP Publishing.)

The Hessian-based predictor-corrector algorithm starts by calculating the energy, gradient and Hessian at the current geometry.[13,17] The classical equations of motion are solved analytically on this local quadratic surface using the vibrational normal modes, like Helgaker and Uggerud's approach.[11,12] The predictor step is integrated for a suitable distance for which the local quadratic surface is a good approximation to the real PES. The energy, gradient and Hessian are calculated at the end of the predictor step, and a fifth order polynomial is fitted to the energy, gradient and Hessian at the beginning and end of the predictor step. A corrector step is taken on this fitted surface using an accurate integration algorithm such as Bulirsch-Stoer. The Hessian calculated at the end of the predictor step also serves as the initial Hessian for the next predictor step (Figure 1). This is a good approximation since the step size is chosen so that the corrector step makes only a small adjustment to the trajectory. Thus, each predictor-corrector step requires only one calculation of the energy, gradient and Hessian. Because the corrector steps greatly improves the accuracy and energy conservation, the step size can be increased by up to an order of magnitude,[17] with a corresponding reduction in the number of electronic structure calculations. The Hessian-based predictor-corrector method has been available in the Gaussian codes for about two decades.

Even though analytic Hessians can be calculated readily, the cost of computing Hessians increases more steeply with molecular size than the cost of gradients. From our work on geometry optimization with quasi-Newton methods,[16] we knew that the Hessian did not need to be calculated at each step, but could be updated using the change in the gradients at each step. The BFGS updating scheme is well suited for finding minima since it keeps the Hessian positive definite. Since trajectories can explore parts of the PES where the Hessian has one or more negative eigenvalues, the update proposed by Bofill is more suitable[18] because it allows for negative eigenvalues in the updated Hessian. We found that the Hessian can be updated for 5−20 steps before it has to be recalculated.[1] A further

https://doi.org/10.1021/acs.accounts.1c00390
Acc. Chem. Res. XXXX, XXX, XXX−XXX

improvement in the Hessian updating method for trajectory calculations was developed by Hase and his group using a compact finite difference approach.[19] For the Bofill update, this amounts to twice the regular update, yielding a Hessian appropriate for the end of the predictor step rather than the middle of the step. With Hessian updating, the cost of second derivative calculations is spread over several steps with the remaining steps requiring only energy and gradient calculations. Estimates show that the Hessian-based predictor-corrector method with updating is more efficient than gradient-based methods for Hartree−Fock calculations on molecules as large as $C_{12}H_{26}$.[1] Recent improvements using reintegration have made the approach even more efficient.[20]

Following a steepest descent path or intrinsic reaction coordinate from the transition state forward to products and back to reactants is very similar to integrating classical trajectories.[16] A steepest descent reaction path can be followed by removing most of the kinetic energy at each step in the trajectory.[21,22] Alternatively, we can used the Hessian-based predictor-corrector approach to integrate the steepest descent equations directly.[23,24] Under favorable circumstances, the Hessian needs to be calculated only at the transition state and can be updated all the way down to reactants and products.

Extended Lagrangian Molecular Dynamics

Gradient-based and Hessian-based methods for classical trajectory calculations are best suited for modest size molecules. In collaboration with Greg Voth and Srini Iyengar (who was a postdoc in the Voth group at the time), we set out to design a direct molecular dynamics method that would be more suitable for larger molecules. In the mid-1980s, Car and Parrinello developed a method for studying materials based on density functional theory and extended Lagrangian dynamics.[25,26] Instead of converging the electronic structure calculations, the orbitals are propagated along with the ions. In Car−Parrinello molecular dynamics (CPMD), plane waves are used represent the electronic structure, the electrons are given a fictitious mass, and the molecular orbitals are propagated classically using an extended Lagrangian. Employing plane waves simplifies many of the integrals but necessitates the use of ultrasoft pseudopotentials (even for light atoms) and limits efficient calculations to pure density functionals. The success of the Car−Parrinello method for materials gave us the idea to develop an extended Lagrangian approach for molecular dynamics with atom-centered basis functions and density matrix propagation,[2,27] termed ADMP. Employing atom-centered basis functions allows us to use existing molecular orbital software to calculate integrals and energy derivatives. No pseudopotentials are needed, and all types of density functionals can be used, including hybrid and range separated functionals that are more accurate than pure functionals. Propagating the density matrix closely resembles the approach used in linear scaling electronic structure calculations,[28] which avoid repeated diagonalizations of the Fock or Kohn−Sham matrices by directly minimizing the energy with respect to variations in the density matrix.

While the classical dynamics of atoms in a molecule are easily described by Newton's equations of motion ($\mathbf{F} = m\mathbf{a}$), the dynamics of the electrons must be constrained so that the density matrix, $\mathbf{P}$, remains idempotent ($\mathbf{PP} = \mathbf{P}$). Constrained dynamics are more easily formulated in terms of the Lagrangian, $L = T - V + \lambda C$, where T is the kinetic energy, V is the potential energy, λ is a Lagrange multiplier, and $C = 0$ is the constraint. By analogy to Car−Parrinello dynamics, we developed an extended Lagrangian method for dynamics of the electron density combined with classical dynamics of the atoms in a molecule.[2,27] The Lagrangian is written as a function of the atomic positions and velocities ($\mathbf{R}$ and $\mathbf{V}$, respectively) and the energy, the density matrix, and its time derivative ($E(\mathbf{R},\mathbf{P})$, $\mathbf{P}$ and $\mathbf{W}$, respectively):

$$L = \frac{1}{2}Tr(\mathbf{V}^T\mathbf{M}\mathbf{V}) + \frac{1}{2}Tr([\boldsymbol{\mu}^{\frac{1}{4}}\mathbf{W}\boldsymbol{\mu}^{\frac{1}{4}}]^2) - E(\mathbf{R}, \mathbf{P}) + Tr(\boldsymbol{\Lambda}(\mathbf{PP} - \mathbf{P})) \quad (1)$$

The first term is the kinetic energy of the atoms ($\mathbf{M}$ is a diagonal matrix of the atomic masses), and the second term is the kinetic energy of the density ($\boldsymbol{\mu}$ is a diagonal matrix of the fictitious mass assigned to the density matrix elements). $E(\mathbf{R},\mathbf{P})$ is obtained from molecular orbital or DFT calculations, and the fourth term is the idempotency constrained on the one electron density matrix so that it properly represents electrons. The energy is calculated using the McWeeny purification of the density, $\mathbf{P} = 3\mathbf{P}^2 - 2\mathbf{P}^3$. The Euler−Lagrange equations of motion for the atoms and the density matrix are

$$\mathbf{M}d^2\mathbf{R}/dt^2 = -\partial E(\mathbf{R}, \mathbf{P})/\partial \mathbf{R}|_{\mathbf{P}}$$
$$\boldsymbol{\mu}^{\frac{1}{2}}\left(d^2\mathbf{P}/dt^2\right)\boldsymbol{\mu}^{\frac{1}{2}} = -\partial E(\mathbf{R}, \tilde{\mathbf{P}})/\partial \mathbf{P}|_{\mathbf{R}} + \boldsymbol{\Lambda}\mathbf{P} + \mathbf{P}\boldsymbol{\Lambda} - \boldsymbol{\Lambda} \quad (2)$$

These equations are propagated using the velocity Verlet algorithm. Instead of solving for the matrix of Lagrange multipliers, $\boldsymbol{\Lambda}$, a simple iterative process ensures that the density matrix is idempotent to 10^{-12} for each step. The propagation starts from a converged electronic structure and is carried out in an orthonormal basis with the transformation obtained by Cholesky decomposition of the overlap matrix. Because the energy is not converged with respect to changes in the density matrix, the formula for the forces on the atoms[2] ($-\partial E/\partial \mathbf{R}$) is somewhat more complicated than that for converged SCF energies; the derivatives of the Cholesky orthonormalization are also needed and are obtained analytically.[2] The ADMP method shows very good energy conservation without the need of thermostats or periodic reconvergence of the electronic structure.[2,27] ADMP has been extended to QM/MM calculations by Rega so that it can be applied to larger biochemical systems.[29]

Molecular Dynamics in Intense Laser Fields

Short, intense laser pulses can rapidly deposit a substantial amount of energy in a molecule, leading to rearrangements and dissociation.[30−32] Laser fields of 10^{14} W cm^{-2} are strong enough to distort the ground state potential energy surface leading to different products than expected from thermal reactions. To improve the accuracy and efficiency of dynamics calculations in intense infrared laser pulses, we have extended our Hessian-based predictor-corrector method to include the time-varying electric field.[33] During a trajectory integration step, the dependence of the forces on the geometry is given by the force constants. The dependence of the forces on the electric field, $\boldsymbol{\varepsilon}(t)$, is given by the dipole and polarizability derivatives.

$$\partial E/\partial \mathbf{R} = \mathbf{g}, \quad \partial E/\partial \boldsymbol{\varepsilon} = -\boldsymbol{\mu}, \quad \partial^2 E/\partial \boldsymbol{\varepsilon}^2 = \boldsymbol{\alpha},$$
$$\partial^2 E/\partial \mathbf{R}\partial \boldsymbol{\varepsilon} = -\partial \boldsymbol{\mu}/\partial \mathbf{R}, \quad \partial^3 E/\partial \mathbf{R}d\boldsymbol{\varepsilon}^2 = -\partial \boldsymbol{\alpha}/\partial \mathbf{R}, \ldots \quad (3)$$

Since they are needed for intensities of infrared and Raman spectra, first derivatives of the dipole and polarizability are

https://doi.org/10.1021/acs.accounts.1c00390
Acc. Chem. Res. XXXX, XXX, XXX−XXX

calculated in most electronic structure codes, whereas higher derivatives are usually not available. With these additional derivatives, the energy can be written as a Taylor expansion in the molecular coordinates and the time-dependent electric field from the laser.

$$\begin{aligned} E(\mathbf{R}, \boldsymbol{\varepsilon}) = {} & E(\mathbf{R}_0, \boldsymbol{\varepsilon}_0) + \partial E/\partial \mathbf{R}(\mathbf{R} - \mathbf{R}_0) \\ & + \frac{1}{2}\partial^2 E/\partial \mathbf{R}^2(\mathbf{R} - \mathbf{R}_0)^2 \\ & + \partial^2 E/\partial \mathbf{R}\partial \boldsymbol{\varepsilon}(\mathbf{R} - \mathbf{R}_0)(\boldsymbol{\varepsilon}(t) - \boldsymbol{\varepsilon}_0) \\ & + \frac{1}{2}\partial^3 E/\partial \mathbf{R}\partial \boldsymbol{\varepsilon}^2(\mathbf{R} - \mathbf{R}_0)(\boldsymbol{\varepsilon}(t) - \boldsymbol{\varepsilon}_0)^2 \end{aligned} \tag{4}$$

The predictor step on this surface is integrated using the velocity Verlet algorithm with a very small step size (no additional electronic structure calculations are needed for this integration).

At the end of the predictor step, another electronic structure calculation is carried out and a surface is fit to the gradients and their derivatives at the beginning and end of the predictor step. We found that a two-point distance weighted interpolant[34] was simpler and more stable than a polynomial interpolation. Some third derivative information can also be included by numerical differentiation of the Hessians obtained at the beginning and end of the predictor step.

$$\begin{aligned} & \mathbf{g}(\mathbf{R}, \boldsymbol{\varepsilon}(t)) = w_1(\mathbf{R})\mathbf{g}_1(\mathbf{R}, \boldsymbol{\varepsilon}(t)) + w_2(\mathbf{R})\mathbf{g}_2(\mathbf{R}, \boldsymbol{\varepsilon}(t)) \\ & w_1(\mathbf{R}) = [1/(\mathbf{R} - \mathbf{R}_1)^2]/[1/(\mathbf{R} - \mathbf{R}_1)^2 + 1/(\mathbf{R} - \mathbf{R}_2)^2] \\ & \mathbf{g}_1(R, \boldsymbol{\varepsilon}(t)) = \mathbf{g}_1(\mathbf{R}_1, \boldsymbol{\varepsilon}(t_1)) + \partial \mathbf{g}_1/\partial \mathbf{R}(\mathbf{R} - \mathbf{R}_1) \\ & \qquad + \frac{1}{2}\partial^2 \mathbf{g}_1/\partial \mathbf{R}^2(\mathbf{R} - \mathbf{R}_1)^2 \\ & \qquad + \partial \mathbf{g}_1/\partial \boldsymbol{\varepsilon}(\boldsymbol{\varepsilon}(t) - \boldsymbol{\varepsilon}_1) \\ & \qquad + \frac{1}{2}\partial^2 \mathbf{g}_1/\partial \boldsymbol{\varepsilon}^2(\boldsymbol{\varepsilon}(t) - \boldsymbol{\varepsilon}_1)^2 \end{aligned} \tag{5}$$

The corrector step is taken on this distance weighted interpolant surface using velocity Verlet. Like the original Hessian-based predictor-corrector method, the electronic structure calculation at the end of the predictor step is used for the start of the next step. Thus, each integration step requires only one electronic structure calculation.

Time-Dependent Configuration Interaction (TDCI) for Electron Dynamics Is Strong Laser Fields

In addition to driving molecular dynamics, strong laser fields can excite and ionize molecules. Through collaborations with Bob Levis and Wen Li, we became interested in strong field ionization caused by ultrashort, intense laser pulses.[35] While the spectroscopy of molecules interacting with weak fields can be treated by perturbation theory, nonadiabatic electron dynamics of molecules in strong laser fields must be simulated by time-dependent methods such as time dependent density functional theory or time-dependent configuration interaction.[32,36−38] There are advantages and disadvantages for each. Since we wanted to simulate single ionization and study the wave function response to strong laser fields, we chose time-dependent configuration interaction with single excitations (TD-CIS).[39] The time-dependent wave function is

$$\begin{aligned} \Psi(t) &= c_0(t)\psi_0 + \sum_{ia} c_i^a(t)\psi_i^a \\ &= C_0(t)\Psi_0 + \sum_{I}^{\text{excited states}} C_I(t)\Psi_I \end{aligned} \tag{6}$$

where ψ_0 and ψ_i^a are the ground and singly excited configurations obtained with the field-free Hamiltonian. Typically, thousands of excited configurations are used for ionization. When compared to EOM-CCSD calculations, we found that CIS and CIS(D) provided a better description of the density of excited states than TD-DFT with typical functionals.[40,41]

The time-dependent Schrodinger equation for the simulation is

$$i\hbar\frac{\partial}{\partial t}\Psi(t) = \hat{\mathbf{H}}(t)\,\Psi(t) = [\hat{\mathbf{H}}_{\text{el}} - \hat{\vec{\mu}}\cdot\vec{E}(t) - i\hat{\mathbf{V}}^{\text{absorb}}]\Psi(t) \tag{7}$$

where $\hat{\mathbf{H}}_{\text{el}}$ is the field-free Hamiltonian. The interaction with the intense laser field is treated in the semiclassical dipole approximation. Ionization is modeled with an absorbing boundary, $\hat{\mathbf{V}}^{\text{absorb}}$, that starts outside the Coulomb barrier. The laser field distorts the molecular electrostatic potential, allowing electron density to escape by passing over the Coulomb barrier or by tunneling through it, Figure 2a. The norm of the wave function decreases as the wave function interacts with the absorbing boundary. The change in the norm squared is taken as

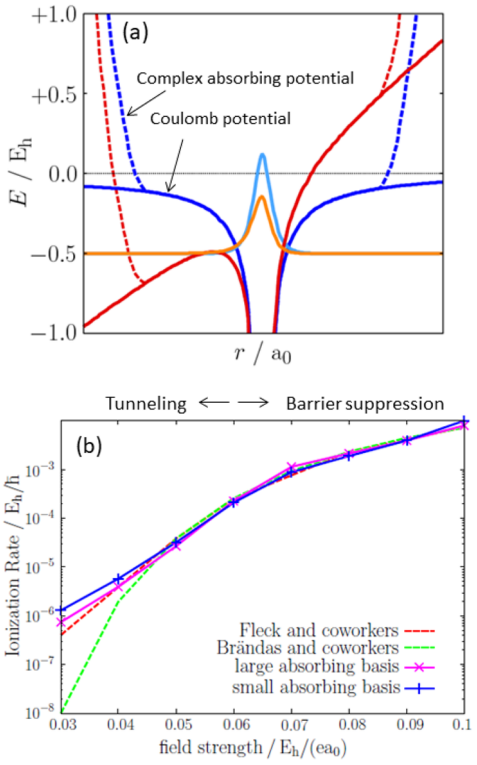

Figure 2. (a) Coulomb potential, complex absorbing potential and ground state wave function for hydrogen atom field-free (blue, dashed blue and light blue) and with a field of 0.06 atomic units (red, dashed red and orange). The field suppresses the Coulomb barrier and the electron can tunnel through the barrier or go over it. (b) TD-CIS ionization rates for hydrogen atom with an absorbing basis set compared to accurate, grid-based calculations. (Adapted with permission from ref 39. Copyright 2014 AIP Publishing.)

https://doi.org/10.1021/acs.accounts.1c00390
Acc. Chem. Res. XXXX, XXX, XXX−XXX

the ionization rate. For static fields greater than 0.04 atomic units, the TD-CIS ionization rates for hydrogen are in good agreement with accurate grid-based calculations,[42,43] Figure 2b.

Like standard molecular orbitals calculations, the TDCI wave function is constructed from orbitals that are linear combinations of atom-centered basis functions. Molecular orbital basis sets such as aug-cc-pVTZ are augmented with extra diffuse Gaussian functions so that the wave function can interact with the absorbing boundary[39] (we typically add four *s*-type, four *p*-type, five *d*-type, and two *f*-type functions to each atom using even tempered exponents down to 0.0032 bohr^{-2}).

The TDCI wave function is propagated using a Trotter−Suzuki factorization of the exponential of the Hamiltonian.

$$\Psi(t + \Delta t) = \exp(-i\hat{\mathbf{H}}\Delta t)\Psi(t)$$

$$\begin{aligned}\mathbf{c}(t + \Delta t) = {} & \exp(-i\mathbf{H}_{el}\Delta t/2)\exp(-\mathbf{V}^{absorb}\Delta t/2) \\ & \times \mathbf{W}^{T}\exp(iE(t + \Delta t/2)\mathbf{d}\Delta t)\mathbf{W} \\ & \times \exp(-\mathbf{V}^{absorb}\Delta t/2)\exp(-i\mathbf{H}_{el}\Delta t/2)\mathbf{c}(t)\end{aligned} \quad (8)$$

Because we use the eigenfunctions of the field-free Hamiltonian, $\exp(-i\mathbf{H}_{el}\Delta t/2)$ is a diagonal matrix. The transition dipole matrix is diagonalized so that the interaction with the time-dependent electric field is easy to calculate. $\mathbf{WDW}^{T} = \mathbf{d}$ are the eigenvalues and eigenvectors of the transition dipole matrix **D** in the field direction. The matrices $\exp(-i\mathbf{H}_{el}\Delta t/2)$, $\exp(-\mathbf{V}^{absorb}\Delta t/2)$, **W**, **d**, and $\mathbf{U} = \exp(-\mathbf{V}^{absorb}\Delta t/2)\mathbf{W}^{T}$ need to be calculated only once at the beginning of the propagation because they are time-independent. A propagation step for a linearly polarized pulse involves two full matrix-vector multiplies (**U** and $\mathbf{U}^{T}$) and three diagonal matrix-vector multiplies ($\exp(-i\mathbf{H}_{el}\Delta t/2)$, $\exp(iE(t + \Delta t/2)\mathbf{d}\Delta t)$, and $\exp(-i\mathbf{H}_{el}\Delta t/2)$. Because the propagation uses the exponential of the Hamiltonian, a fairly large time step of Δt = 0.05 au (1.2 as) can be used with no loss of accuracy.[44]

Circularly polarized pulses can be handled by a modification of the Trotter factorization.[45] Strong field ionization of open shell systems can be simulated with spin-unrestricted wave functions. As an alternative, we have implemented TD-CISD-IP[46] using the CISD-IP approach of Krylov which builds cation wave functions from singly ionized configurations of the neutral and singly excited, singly ionized configurations.[47] We have also extended the code to include spin−orbit coupling in TD-CIS and TD-CISD-IP simulations of strong field ionization.[48]

APPLICATIONS OF DIRECT DYNAMICS

Born−Oppenheimer Molecular Dynamics

One of the first ab initio direct dynamics application was by Helgaker and Uggerud in the early 1990s to study $CH_2OH^+ \rightarrow HCO^+ + H_2$.[11,12] Our applications of ab initio molecular dynamics began as a collaboration with Hase on the dissociation of $CH_2O \rightarrow H_2 + CO$.[13] Because our computer resources in the mid-1990s were rather limited and we needed 400 trajectories for reasonable statistics, the electronic structure calculations were restricted to Hartree−Fock theory. Nevertheless, the agreement with the experimental vibrational distribution for the products was very good, Table 1. The next collaborative direct dynamics study looked at $H + C_2H_4$ and $F + C_2H_4$.[49] An ensemble average of trajectories for $F + C_2H_4$ initiated at the exit channel barrier yielded a broad product translational energy distribution, similar to experiment.[50] Hase and his group have used direct dynamics extensively to investigate many aspects of molecular dynamics.

Table 1. Vibrational Distribution for Photofragments CO and H_2

	CO		H_2	
v	HF/6-31G(d,)	expt[a]	HF/6-31G(d,p)	expt[b]
0	82.2%	88%	22.8%	24.2%
1	17.8%	12%	36.5%	41.3%
2			27.0%	24.6%
3			11.2%	8.6%
4			2.5%	0.3%

[a]From ref 91. [b]From ref 92 (adapted with permission from ref 13 Copyright 1994 Elsevier).

By 2002, MP2 second derivatives were available, computer resources were more abundant, and Hessian updating improved the efficiency of trajectory calculations. This allowed us to use the MP2/6-31G(d,p) level of theory to examine the effect of substituents on XCHO → HX + CO (X = H, F, Cl).[51] In all three cases, CO is produced rotationally hot but vibrationally cold. HCl shows significantly more vibrational excitation than H_2 and HF. The energy partitioning for FCHO showed good qualitative agreement with experiment;[52] no experiments were available for ClCHO.

Direct dynamics calculations are particularly advantageous for studying reactions where the path branches after the transition state. In collaboration with Sason Shaik, we used reaction path following and ab initio molecular dynamics to examine reactions in which a single transition serves two mechanisms,[53−55] Figure 3. A ketyl radical anion can react with an alkyl halide either by S_N2 substitution at carbon, Sub(C), or by inner-sphere electron transfer, ET, via the same transition state (a third path, S_N2 at oxygen, Sub(O), proceeds through a separate transition state). Ab initio classical trajectory calculations with Hartree−Fock and DFT were used to study the branching ratios as a function of substituents and temperature. Our direct dynamics studies show that Sub(C) products are favored for transition states with short C−C bonds and ET for long C−C bonds. Higher temperatures favored ET products produced either directly or through dissociation of Sub(C) products.

Photodissociation of glyoxal, $C_2H_2O_2$, has a three-body dissociation channel, $C_2H_2O_2 \rightarrow 2CO + H_2$, as well as a two-body channel, $CH_2O + H_2$.[56] We have investigated the dynamics of glyoxal dissociation with Hartree−Fock and density functional theory.[57−59] For both channels, CO had a broad rotational distribution but very little vibrational excitation, in accord with experiment.[60] Both H_2 and CH_2O had significant vibrational excitation.[56] The photodissociation of *s*-tetrazine also proceeds via a three-body fragmentation channel,[61] $C_2N_4H_2 \rightarrow 2HCN + N_2$. Our direct dynamics calculations produced HCN with a very broad rotational distribution and extensive excitation of the bending vibration.[62] By contrast, N_2 was produced rotationally cold and with only a small amount of vibrational excitation in agreement with experiment.

The nonstatistical dissociation of acetone radical cation has been the subject of a number of experimental and theoretical studies.[63,64] The enol, generated via the McLafferty rearrangement, can isomerize to the keto form resulting in chemical activation of the newly formed methyl group. Our direct dynamics calculations show that the active methyl group dissociates earlier and with more translational energy than the spectator group.[65] The branching ratio depends on the rate of

https://doi.org/10.1021/acs.accounts.1c00390
Acc. Chem. Res. XXXX, XXX, XXX−XXX

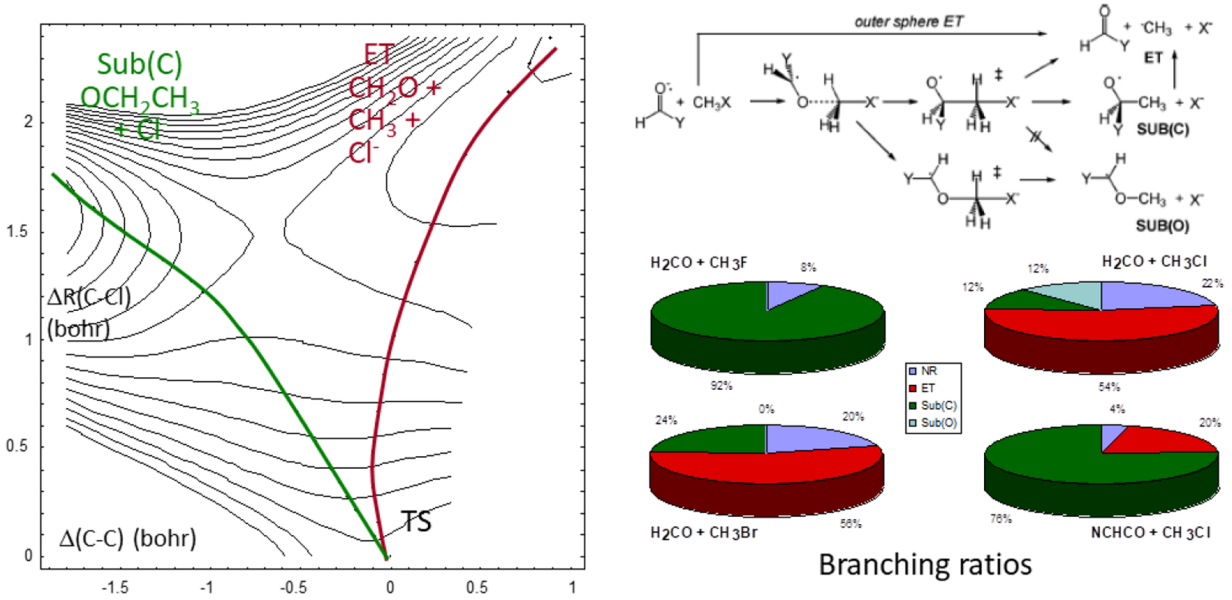

Figure 3. A single transition serves two mechanisms: The reaction path bifurcates after the transition state, leading to S_N2 substitution at carbon, Sub(C), and inner-sphere electron transfer, ET. The branching ratios vary with the substituent on the ketyl radical anion and the alkyl halide. (Adapted with permission from ref 53. Copyright 2001 American Chemical Society.)

energy redistribution in the chemically activated molecule and ranges from 1.4 to 1.9, depending on the excess energy of the transition state. This branching ratio can be enhanced by exciting vibrational modes that involve C−C−O bending.The

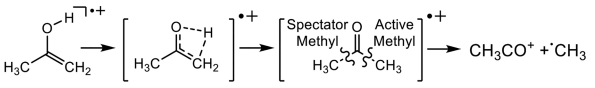

(9)

flow of energy in a chemically activated molecule can be seen more dramatically in pentanedione radical cation. The bond dissociation energies for two interior C−C bonds are equal and 7−8 kcal/mol lower than the exterior C−C bonds. Our direct dynamics calculations show a very large deviation from statistical behavior, with the dissociation of the C−C bond closer to the activated methyl group 20 times greater than the more distant interior C−C bond.[66]

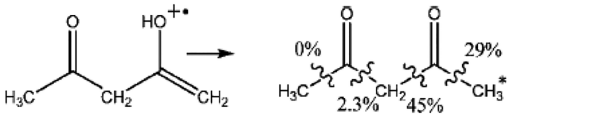

(10)

The 1,3-cyclobutanedione radical cation is an analogous system that has four equivalent C−C bonds. The majority of the trajectories yielded CH_2CO^+ + CH_2CO. The dissociation is nonstatistical with the activated C−C bond breaking twice as often as the spectator C−C bond.[67]

Strong Field Molecular Dynamics

Intense laser pulses can quickly deposit large amounts of energy in a molecule and produce multiply charged ions.[30−32] When many electrons are removed, bonds are severely weakened and molecules dissociate readily by Coulomb explosion.[31,32,68] If only a few electrons are ionized, there may still be significant barriers and multiple pathways for dissociation on the ground state PES are possible. We have used direct dynamics to study the dissociation of acetylene dication with excess internal

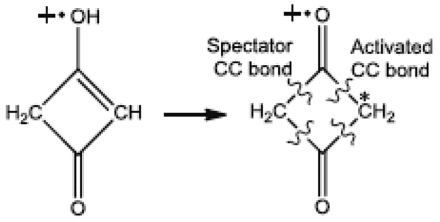

(11)

energy.[69] Direct deprotonation yielding HCC^+ + H^+ is the dominant path. Deprotonation after isomerization to H_2CC^{2+} is also seen. Similarly, deprotonation is the major pathway for CH_2NH^+ and $CHNH_2^{2+}$.[70] Allene dication has a much richer potential energy surface.[71−73] Direct dynamics on the lowest singlet and triplet PES show isomerizations to propyne and cyclopropane dications.[73] Deprotonation from each of these isomers is the major pathway, but loss of CH_2^+ and H_2^+ are also seen.

Intense infrared laser pulses can distort the ground state PES and drive dynamics during the pulse. For example, an intense IR field aligned with a bond, depresses the bond dissociation potential.[74] For HCO^+ in an intense 10 μm CW laser field, we found that the C−H bond dissociates rapidly when the field is aligned with the molecular axis (Figure 4, red).[75] When the field polarization is perpendicular, the dissociation is delayed while molecule rotates into the field direction (Figure 4, blue).

If a molecule has several dissociation channel, orientating the molecule in the laser field can favor one dissociation path over others. Formyl chloride cation in a 7 μm linearly polarized pulse is one example that we have studied by direct dynamics,[3] Figure 5. Dissociation to Cl + HCO^+ is the lowest energy path and is favored when averaged over all orientations. The two higher energy channels, H + CO^+ and HCl^+ + CO, can be greatly enhanced when the laser polarization is aligned with the C−H bond or perpendicular to the C−H bond, respectively. We have also examined $ClCHO^+$ dissociation with pairs linearly polarized

https://doi.org/10.1021/acs.accounts.1c00390
Acc. Chem. Res. XXXX, XXX, XXX−XXX

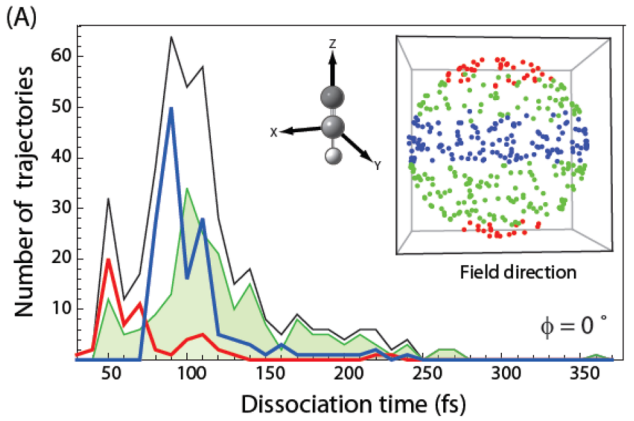

Figure 4. Dissociation times for HCO^+ in an intense 10 μm CW laser field. The electric fields were applied in random orientations (see insets). Red curves and dots correspond to small angles with respect to the molecular axis, green for intermediate angles, and blue for nearly perpendicular orientations. (Reproduced with permission from ref 75. Copyright 2012 Elsevier.)

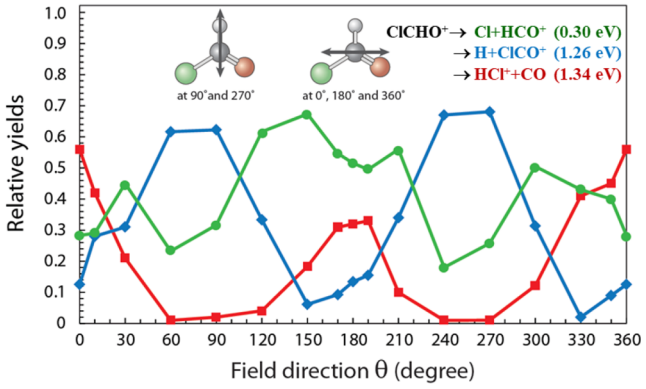

Figure 5. Relative yield of $ClCHO^+$ dissociation into Cl + HCO^+ (green), H + $ClCO^+$ (blue), and HCl^+ + CO (red) as a function of the orientation of the laser field. (Reproduced with permission from ref 3. Copyright 2012 American Chemical Society.)

pulse with different orientations and wavelengths and with circularly polarized pulses.[76,77]

While it may be difficult to orient $ClHCO^+$ in practice, molecules like CF_3Br and C_6H_5I can be aligned experimentally. Our simulations show that selective dissociation of C−F over C−Br can be achieved when the polarization of the laser pulse is aligned with the C−F bond in CF_3Br^+.[78] Likewise, C−H dissociation is favored in $C_6H_5I^{2+}$ when the polarization is perpendicular to the C−I bond. We have also carried out direct dynamics calculations of $CH_3NH_2^+$, CH_3OH^+, CH_3F^+, and $C_3H_4^+$ aligned in 7 μm laser pulses.[79−82] Compared to random orientations, CH_3X^+ with C−X aligned with the laser polarization gained nearly twice as much energy from laser fields, increasing the percentage of C−X dissociation. Alignment also increased the branching ratio for H_2 elimination in $CH_3NH_2^+$ and CH_3OH^+ and for isomerization in CH_3OH^+.

Strong Field Electron Dynamics

Intense laser fields can drive electron dynamics causing excitations and ionization. Strong electric fields depresses the Coulomb barrier and an electron can tunnel through the barrier or go over it on a time scale that is much shorter than molecular dynamics.[30−32,35−39] TD-CIS simulations are well suited to model barrier suppression ionization by intense, ultrashort 800 nm pulses. Similar to molecular dynamics in intense laser fields, there is a strong angular dependence for the ionization rates.

Figure 6 shows the angular dependence of the ionization rate for oxygen molecule.[4] At the lowest intensity, ionization is

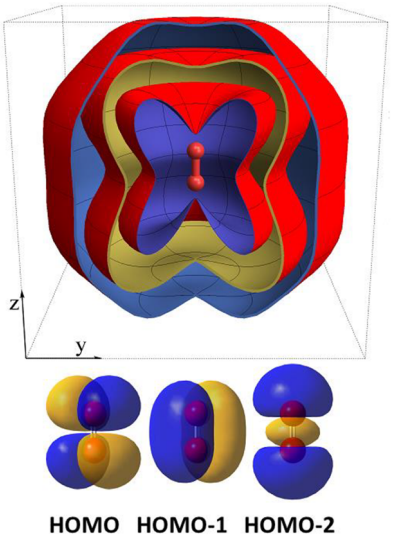

Figure 6. Angle dependence of ionization for O_2 calculated with TDCI for three different intensities of a seven cycle 800 nm linearly polarized pulse. The ionization yield is plotted radially ,and the angle corresponds to the direction of polarization of the field. The three highest occupied orbitals O_2 are shown. (Adapted with permission from ref 4. Copyright 2015 American Chemical Society.)

mainly from the highest occupied molecular orbital (HOMO) which has a node along the molecular axis and a node perpendicular to it. The maxima and minima in the ionization yield follow the shape of the HOMO. At higher intensities, electrons are also ionized from HOMO-1 and HOMO-2, increasing the ionization yield perpendicular and parallel to the molecular axis, respectively.

Population analysis of the absorbed wave function can be used to partition the total ionization yield into contributions from individual orbitals, as shown in Figure 7 for water.[83] Perpendicular to the molecular plane (x-axis), ionization is dominated by the π-type lone pair (HOMO) for all intensities; along the C_2 axis (z-axis), the ionization yield is much smaller and is from the σ-type lone pair (HOMO-1). We found a similar correspondence between the angular dependence of the ionization yield and the shapes of the highest two or three molecular orbitals for other second and third period hydrides (AH_n, A = B−F, Al−Cl)[83] and a variety of triply bonded species.[84]

Many of the studies with intense laser pulses are carried out with elliptical or circularly polarized light. TD-CIS simulations of the angular dependence of ionization of formaldehyde are shown in Figure 8 for linearly and circularly polarized pulses.[45] In a circularly polarized pulse, the electric field rotates about the direction of propagation. When the results for linearly polarized light, Figure 8b, are averaged over rotation about the axis of propagation, Figure 8c, the angular dependence is very similar to that calculated directly for circularly polarized light, Figure 8a. Thus, the shape of the ionization yield with circularly polarized light can be modeled with the results for linearly polarized light

https://doi.org/10.1021/acs.accounts.1c00390
Acc. Chem. Res. XXXX, XXX, XXX−XXX

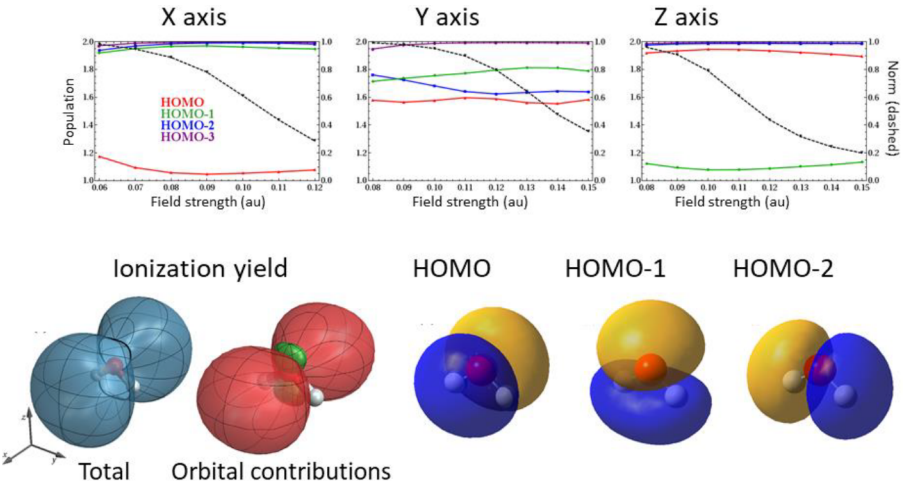

Figure 7. Populations of the absorbed wave function for laser polarizations in the *x*-, *y*-, and *z*-directions. Total ionization yield for H_2O and contributions from HOMO (red), HOMO-1 (green), and HOMO-2 (blue). (Adapted with permission from ref 83. Copyright 2015 American Chemical Society.)

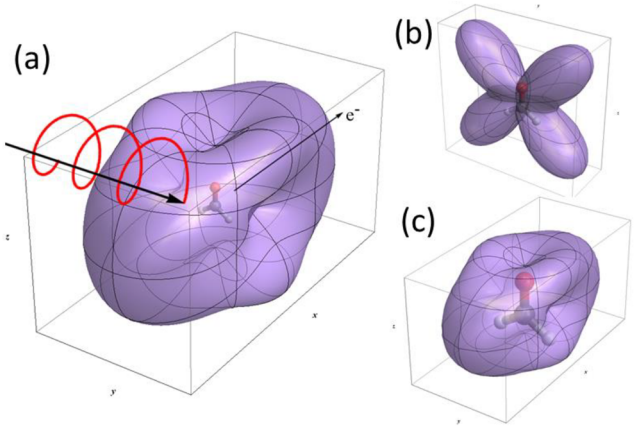

Figure 8. Angular dependence of ionization of CH_2O: (a) circularly polarized laser pulse, with ionization yield plotted radially in the direction of propagation of the pulse, (b) linearly polarized laser pulse, with ionization yield plotted radially in the direction of polarization of the pulse, and (c) rotational average of the ionization yield for linearly polarized light. (Adapted with permission from ref 45. Copyright 2017 American Chemical Society.)

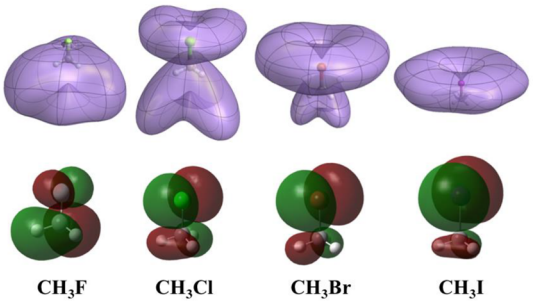

Figure 9. Angular dependence of the ionization yield for methyl halides using a static field and the highest occupied molecular orbitals for the methyl halides. (Adapted with permission from ref 44. Copyright 2017 American Chemical Society.)

which can be understood in terms of the nodal properties of the highest 2 or 3 molecular orbitals.

Strong field angular streaking experiments involving the detection of ions and electrons in coincidence and the measurement of their momenta have been used to determine angle-dependent ionization yields.[85] These methods applied to CH_3I are able to distinguish ionization from the iodine side and the methyl side of the molecule. To obtain similar angular information, we used TDCI calculations with a static field to simulate ionization of the series of methyl halides,[44] Figure 9. Because fluorine is very electronegative and binds electrons tightly, CH_3F ionizes mainly from the methyl group; CH_3Cl and CH_3Br show ionization from both the methyl group and the halogen; and CH_3I ionizes mainly from the p_π orbitals of the iodine. Similar results have been obtained for haloacetylenes,[86] HCCX (X = F, Cl, Br, I). HCCF ionizes primarily from the CC π-bond with no contribution from F, while HCCI ionizes mainly from I with a small component from the CC π-bond. Strong field ionization of 2-phenylethyl-*N*,*N*-dimethylamine (PENNA) is the largest system that we have studied to date with TD-CIS.[87]

Intense laser pulses can cause multiple ionizations. Sequential double ionization can dominate for over-the-barrier ionization.[88,89] We have modeled sequential double ionization by running two TDCI simulations in tandem[90] (Figure 10). The first simulation uses TD-CIS[39] to ionize a neutral molecule. At each time step, the newly ionized part of the wave function from the first simulation is fed into a second simulation for ionizing the cation to the dication using TD-CISD-IP.[46]

■ OUTLOOK

Over the past 25 years, ab initio molecular dynamics has developed into a powerful method for exploring potential energy surfaces for chemical reactions. Steady advances in computer hardware and computational chemistry software have made this methodology more affordable and widely applicable for reactions on ground state potential energy surfaces. In addition to the usual challenges encountered in traditional classical trajectory studies on analytic potential energy surfaces, "on-the-fly" direct dynamics calculations require electronic structure methods that are sufficiently fast and accurate for the systems under investigation. Nuclear quantum effects may be important in systems with light atoms and can be treated with path integral methods. Most often these methods are carried out on fitted potential energy surfaces, but increasingly they are being

https://doi.org/10.1021/acs.accounts.1c00390
Acc. Chem. Res. XXXX, XXX, XXX−XXX

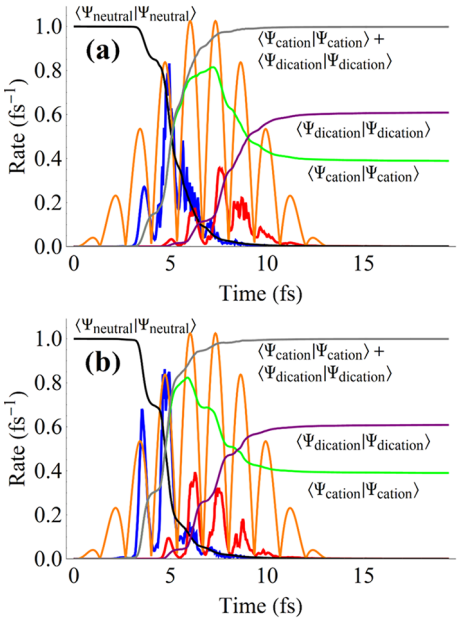

Figure 10. Sequential double ionization of HBr by an intense, linearly polarized pulse with the polarization directions aligned (a) parallel and (b) perpendicular to the molecular axis: blue, ionization rate for the neutral; red, ionization rate for the cation; 6 times the absolute value of the electric field is shown in orange. (Reproduced with permission from ref 90. Copyright 2021 AIP Publishing.)

extended to direct dynamics calculations. Molecular dynamics simulations for excited states are much more difficult than adiabatic classical dynamics for ground states. Excited state electronic structure methods must describe the interaction of several excited states on an equal footing and include an adequate treatment of electron correlation. Developing computational efficient methods for excited state direct dynamics is an active area of research. To account for transitions between excited states during the simulations, nonadiabatic effects must be included. Developments in this area are discussed in other Accounts in this special issue. Strong field chemistry has an added complication in that simulations may need to include direct coupling between electron and nuclear dynamics during the intense laser pulse. This is another area of active research with significant challenges.

AUTHOR INFORMATION

Corresponding Author

H. Bernhard Schlegel − *Department of Chemistry, Wayne State University, Detroit, Michigan 48202, United States;* orcid.org/0000-0001-7114-2821; Email: hbs@chem.wayne.edu; Fax: 313-577-8822

Complete contact information is available at: https://pubs.acs.org/10.1021/acs.accounts.1c00390

Notes

The author declares no competing financial interest.

Biography

H. Bernhard Schlegel received his BSc from University of Waterloo in 1972 and PhD from Queen's University, Canada in 1975, studying theoretical organic chemistry with Prof. Saul Wolfe. His postdoctoral research was with Kurt Mislow and Lee Allen at Princeton, 1976−77, and with John Pople at Carnegie-Mellon University, 1977−78. He was a senior research chemist at Merck, Sharp & Dohme Research Laboratories before accepting a faculty appointment in Chemistry at Wayne State University in 1980. He is currently Distinguished Professor of Chemistry, Emeritus, at Wayne State. U.

ACKNOWLEDGMENTS

This work was supported by grants from the National Science Foundation (most recently CHE1856437). Some of the work on strong field chemistry in collaboration with Wen Li has been supported by DOE (recently DE-SC0020994). The author would like to thank all of the collaborators, postdoctoral fellows, and graduate students involved in the research summarized in this Account.

REFERENCES

(1) Bakken, V.; Millam, J. M.; Schlegel, H. B. Ab initio classical trajectories on the Born-Oppenheimer surface: Updating methods for Hessian-based integrators. *J. Chem. Phys.* **1999**, *111*, 8773−8777.
(2) Schlegel, H. B.; Millam, J. M.; Iyengar, S. S.; Voth, G. A.; Daniels, A. D.; Scuseria, G. E.; Frisch, M. J. Ab initio molecular dynamics: Propagating the density matrix with Gaussian orbitals. *J. Chem. Phys.* **2001**, *114*, 9758−9763.
(3) Lee, S. K.; Suits, A. G.; Schlegel, H. B.; Li, W. A reaction accelerator: Mid-infrared strong field dissociation yields mode-selective chemistry. *J. Phys. Chem. Lett.* **2012**, *3*, 2541−2547.
(4) Krause, P.; Schlegel, H. B. Angle-dependent ionization of small molecules by time-dependent configuration interaction and an absorbing potential. *J. Phys. Chem. Lett.* **2015**, *6*, 2140−2146.
(5) Bunker, D. L. Classical Trajectory Methods. *Methods Comput. Phys.* **1971**, *10*, 287.
(6) Raff, L. M.; Thompson, D. L. The classical trajectory approach to reactive scattering,. In *Theory of Chemical Reaction Dynamics*; Baer, M., Ed.; CRC Press: Boca Raton, FL, 1985.
(7) Schatz, G. C. The analytical representation of potential energy surfaces. *Rev. Mod. Phys.* **1989**, *61*, 669−688.
(8) Hollebeek, T.; Ho, T. S.; Rabitz, H. Constructing multidimensional molecular potential energy surfaces from ab initio data. *Annu. Rev. Phys. Chem.* **1999**, *50*, 537−570.
(9) Wang, I. S. Y.; Karplus, M. Dynamics of organic reactions. *J. Am. Chem. Soc.* **1973**, *95*, 8160−8164.
(10) Leforestier, C. Classical trajectories using full abinitio potential-energy surface $H^- + CH_4 \rightarrow CH_{4+}H^-$. *J. Chem. Phys.* **1978**, *68*, 4406−4410.
(11) Helgaker, T.; Uggerud, E.; Jensen, H. J. A. Integration of the classical equations of motion on ab initio molecular-potential energy surfaces using gradients and hessians - Application to translational energy-release upon fragmentation. *Chem. Phys. Lett.* **1990**, *173*, 145−150.
(12) Uggerud, E.; Helgaker, T. Dynamics of the reaction $CH_2OH^+ \rightarrow CHO^+ + H_2$ - translational energy-release from abinitio trajectory calculations. *J. Am. Chem. Soc.* **1992**, *114*, 4265−4268.
(13) Chen, W.; Hase, W. L.; Schlegel, H. B. Ab-initio classical trajectory study of $H_2CO \rightarrow H_2+CO$ dissociation. *Chem. Phys. Lett.* **1994**, *228*, 436−442.
(14) Pople, J. A.; Krishnan, R.; Schlegel, H. B.; Binkley, J. S. Derivative studies in Hartree-Fock and Møller-Plesset theories. *Int. J. Quantum Chem.* **1979**, *16*, 225−241.
(15) Schlegel, H. B. Analytical 2nd derivatives of 2 electron integrals over s and p Cartesian Gaussians. *J. Chem. Phys.* **1989**, *90*, 5630−5634.
(16) Schlegel, H. B. Geometry optimization. *Wiley Interdiscip. Rev.: Comput. Mol. Sci.* **2011**, *1*, 790−809.
(17) Millam, J. M.; Bakken, V.; Chen, W.; Hase, W. L.; Schlegel, H. B. Ab initio classical trajectories on the Born-Oppenheimer surface: Hessian-based integrators using fifth-order polynomial and rational function fits. *J. Chem. Phys.* **1999**, *111*, 3800−3805.

(18) Bofill, J. M. Updated hessian matrix and the restricted step method for locating transition structures. *J. Comput. Chem.* **1994**, *15*, 1−11.
(19) Wu, H.; Rahman, M.; Wang, J.; Louderaj, U.; Hase, W. L.; Zhuang, Y. Higher-accuracy schemes for approximating the Hessian from electronic structure calculations in chemical dynamics simulations. *J. Chem. Phys.* **2010**, *133*, 074101.
(20) Zheng, J.; Frisch, M. J. Re-integration with anchor points algorithm for ab initio molecular dynamics. *J. Chem. Phys.* **2021**, *155*, 074106.
(21) Maluendes, S. A.; Dupuis, M. A dynamic reaction coordinate approach to abinitio reaction pathways - application to the 1,5 hexadiene cope rearrangement. *J. Chem. Phys.* **1990**, *93*, 5902−5911.
(22) Hratchian, H. P.; Schlegel, H. B. Following reaction pathways using a damped classical trajectory algorithm. *J. Phys. Chem. A* **2002**, *106*, 165−169.
(23) Hratchian, H. P.; Schlegel, H. B. Using Hessian updating to increase the efficiency of a Hessian based predictor-corrector reaction path following method. *J. Chem. Theory Comput.* **2005**, *1*, 61−69.
(24) Hratchian, H. P.; Frisch, M. J.; Schlegel, H. B. Steepest descent reaction path integration using a first-order predictor−corrector method. *J. Chem. Phys.* **2010**, *133*, 224101.
(25) Car, R.; Parrinello, M. Unified approach for molecular-dynamics and density-functional theory. *Phys. Rev. Lett.* **1985**, *55*, 2471−2474.
(26) Hutter, J. Car-Parrinello molecular dynamics. *Wiley Interdiscip. Rev.-Comput. Mol. Sci.* **2012**, *2*, 604−612.
(27) Iyengar, S. S.; Schlegel, H. B.; Millam, J. M.; Voth, G. A.; Scuseria, G. E.; Frisch, M. J. Ab initio molecular dynamics: Propagating the density matrix with Gaussian orbitals. II. Generalizations based on mass-weighting, idempotency, energy conservation and choice of initial conditions. *J. Chem. Phys.* **2001**, *115*, 10291−10302.
(28) Millam, J. M.; Scuseria, G. E. Linear scaling conjugate gradient density matrix search as an alternative to diagonalization for first principles electronic structure calculations. *J. Chem. Phys.* **1997**, *106*, 5569−5577.
(29) Rega, N.; Iyengar, S. S.; Voth, G. A.; Schlegel, H. B.; Vreven, T.; Frisch, M. J. Hybrid ab-initio/empirical molecular dynamics: Combining the ONIOM scheme with the atom-centered density matrix propagation (ADMP) approach. *J. Phys. Chem. B* **2004**, *108*, 4210−4220.
(30) Corkum, P. B.; Ivanov, M. Y.; Wright, J. S. Subfemtosecond processes in strong laser fields. *Annu. Rev. Phys. Chem.* **1997**, *48*, 387−406.
(31) Posthumus, J. H. The dynamics of small molecules in intense laser fields. *Rep. Prog. Phys.* **2004**, *67*, 623−665.
(32) Nisoli, M.; Decleva, P.; Calegari, F.; Palacios, A.; Martin, F. Attosecond electron dynamics in molecules. *Chem. Rev.* **2017**, *117*, 10760−10825.
(33) Schlegel, H. B. Molecular dynamics in strong laser fields: A new algorithm for ab initio classical trajectories. *J. Chem. Theory Comput.* **2013**, *9*, 3293−3298.
(34) Ischtwan, J.; Collins, M. A. Molecular potential energy surfaces by interpolation. *J. Chem. Phys.* **1994**, *100*, 8080−8088.
(35) Ivanov, M. Y.; Spanner, M.; Smirnova, O. Anatomy of strong field ionization. *J. Mod. Opt.* **2005**, *52*, 165−184.
(36) Goings, J. J.; Lestrange, P. J.; Li, X. Real-time time-dependent electronic structure theory. *Wiley Interdiscip. Rev.: Comput. Mol. Sci.* **2018**, *8*, e1341.
(37) Palacios, A.; Martin, F. The quantum chemistry of attosecond molecular science. *Wiley Interdiscip. Rev.: Comput. Mol. Sci.* **2020**, *10*, e1430.
(38) Ishikawa, K. L.; Sato, T. A review on ab initio approaches for multielectron dynamics. *IEEE J. Sel. Top. Quantum Electron.* **2015**, *21*, 8700916.
(39) Krause, P.; Sonk, J. A.; Schlegel, H. B. Strong field ionization rates simulated with time-dependent configuration interaction and an absorbing potential. *J. Chem. Phys.* **2014**, *140*, 174113.
(40) Sonk, J. A.; Caricato, M.; Schlegel, H. B. TD-CI Simulation of the Electronic Optical Response of Molecules in Intense Fields: Comparison of RPA, CIS, CIS(D), and EOM-CCSD. *J. Phys. Chem. A* **2011**, *115*, 4678−4690.
(41) Sonk, J. A.; Schlegel, H. B. TD-CI Simulation of the Electronic Optical Response of Molecules in Intense Fields II: Comparison of DFT Functionals and EOM-CCSD. *J. Phys. Chem. A* **2011**, *115*, 11832−11840.
(42) Hermann, M. R.; Fleck, J. A. Split-operator spectral method for solving the time-dependent Schrodinger-equation in spherical coordinates. *Phys. Rev. A: At., Mol., Opt. Phys.* **1988**, *38*, 6000−6012.
(43) Hehenberger, M.; McIntosh, H. V.; Brandas, E. Weyls theory applied to stark effect in hydrogen-atom. *Phys. Rev. A: At., Mol., Opt. Phys.* **1974**, *10*, 1494−1506.
(44) Hoerner, P.; Schlegel, H. B. Angular dependence of strong field ionization of CH_3X (X = F, Cl, Br, or I) using time-dependent configuration interaction with an absorbing potential. *J. Phys. Chem. A* **2017**, *121*, 5940−5946.
(45) Hoerner, P.; Schlegel, H. B. Angular dependence of ionization by circularly polarized light calculated with time-dependent configuration interaction with an absorbing potential. *J. Phys. Chem. A* **2017**, *121*, 1336−1343.
(46) Lee, M. K.; Li, W.; Schlegel, H. B. Angular dependence of strong field sequential double ionization for neon and acetylene simulated with time-dependent configuration interaction using CIS and CISD-IP. *J. Chem. Phys.* **2020**, *152*, 064106.
(47) Golubeva, A. A.; Pieniazek, P. A.; Krylov, A. I. A new electronic structure method for doublet states: Configuration interaction in the space of ionized 1h and 2h1p determinants. *J. Chem. Phys.* **2009**, *130*, 124113.
(48) Lee, M. K.; Hoerner, P.; Li, W.; Schlegel, H. B. Effect of spin-orbit coupling on strong field ionization simulated with time-dependent configuration interaction. *J. Chem. Phys.* **2020**, *153*, 244109.
(49) Bolton, K.; Schlegel, H. B.; Hase, W. L.; Song, K. Y. An ab initio quasi-classical direct dynamics investigation of the $F+C_2H_4 \rightarrow C_2H_3F+H$ product energy distributions. *Phys. Chem. Chem. Phys.* **1999**, *1*, 999−1011.
(50) Robinson, G. N.; Continetti, R. E.; Lee, Y. T. The translational energy-dependence of the $F+C_2H_4 \rightarrow H+C_2H_3F$ reaction cross-section near threshold. *J. Chem. Phys.* **1990**, *92*, 275−284.
(51) Anand, S.; Schlegel, H. B. Unimolecular dissociation of formyl halides HXCO → CO+HX (X = F, Cl): An ab initio direct classical trajectory study. *J. Phys. Chem. A* **2002**, *106*, 11623−11629.
(52) Choi, Y. S.; Moore, C. B. State-specific unimolecular dissociation dynamics of HFCO. 2. CO rotational distribution and doppler widths. *J. Chem. Phys.* **1995**, *103*, 9981−9988.
(53) Bakken, V.; Danovich, D.; Shaik, S.; Schlegel, H. B. A single transition state serves two mechanisms: An ab initio classical trajectory study of the electron transfer and substitution mechanisms in reactions of ketyl radical anions with alkyl halides. *J. Am. Chem. Soc.* **2001**, *123*, 130−134.
(54) Li, J.; Li, X.; Shaik, S.; Schlegel, H. B. Single transition state serves two mechanisms. Ab initio classical trajectory calculations of the substitution-electron transfer branching ratio in $CH_2O^- + CH_3Cl$. *J. Phys. Chem. A* **2004**, *108*, 8526−8532.
(55) Li, J.; Shaik, S.; Schlegel, H. B. A single transition state serves two mechanisms. The branching ratio for $CH_2O^- + CH_3Cl$ on improved potential energy surfaces. *J. Phys. Chem. A* **2006**, *110*, 2801−2806.
(56) Dobeck, L. M.; Lambert, H. M.; Kong, W.; Pisano, P. J.; Houston, P. L. H_2 production in the 440-nm photodissociation of glyoxal. *J. Phys. Chem. A* **1999**, *103*, 10312−10323.
(57) Li, X.; Schlegel, H. B. Photodissociation of glyoxal: Resolution of a paradox. *J. Chem. Phys.* **2001**, *114*, 8−10.
(58) Li, X.; Millam, J. M.; Schlegel, H. B. Glyoxal photodissociation. An ab initio direct classical trajectory study of $C_2H_2O_2 \rightarrow H_2+2$ CO. *J. Chem. Phys.* **2001**, *114*, 8897−8904.
(59) Li, X.; Millam, J. M.; Schlegel, H. B. Glyoxal photodissociation. II. An ab initio direct classical trajectory study of $C_2H_2O_2 \rightarrow CO+H_2CO$. *J. Chem. Phys.* **2001**, *115*, 6907−6912.

https://doi.org/10.1021/acs.accounts.1c00390
Acc. Chem. Res. XXXX, XXX, XXX−XXX

(60) Burak, I.; Hepburn, J. W.; Sivakumar, N.; Hall, G. E.; Chawla, G.; Houston, P. L. State-to-state photodissociation dynamics of *trans*-glyoxal. *J. Chem. Phys.* **1987**, *86*, 1258−1268.
(61) Windisch, V. L.; Smith, A. B.; Hochstrasser, R. M. Unimolecular photodissociation of s-tetrazine and derivatives. *J. Phys. Chem.* **1988**, *92*, 5366−5370.
(62) Li, X.; Anand, S.; Millam, J. M.; Schlegel, H. B. An ab initio direct classical trajectory study of s-tetrazine photodissociation. *Phys. Chem. Chem. Phys.* **2002**, *4*, 2554−2559.
(63) Osterheld, T. H.; Brauman, J. I. Infrared multiple-photon dissociation of the acetone enol radical-cation - dependence of nonstatistical dissociation on internal energy. *J. Am. Chem. Soc.* **1993**, *115*, 10311−10316.
(64) McAdoo, D. J. Contributions of $C_3H_6O^{+\cdot}$ ions with the oxygen on the middle carbon to gas phase ion chemistry. *Mass Spectrom. Rev.* **2000**, *19*, 38−61.
(65) Zhou, J.; Schlegel, H. B. Dissociation of acetone radical cation ($CH_3COCH_3^{+\cdot} \rightarrow CH_3CO+ + CH_3\cdot$): An ab initio direct classical trajectory study of the energy dependence of the branching ratio. *J. Phys. Chem. A* **2008**, *112*, 13121−13127.
(66) Zhou, J.; Schlegel, H. B. Large nonstatistical branching ratio in the dissociation of pentane-2,4-dione radical cation: An ab initio direct classical trajectory study. *J. Phys. Chem. A* **2009**, *113*, 1453−1458.
(67) Zhou, J.; Schlegel, H. B. Ab initio classical trajectory calculations of 1,3-cyclobutanedione radical cation dissociation. *Theor. Chem. Acc.* **2012**, *131*, 1126.
(68) Vager, Z.; Naaman, R.; Kanter, E. P. Coulomb explosion imaging of small molecules. *Science* **1989**, *244*, 426−431.
(69) Li, X.; Schlegel, H. B. Ab initio classical trajectory calculations of acetylene dication dissociation. *J. Phys. Chem. A* **2004**, *108*, 468−472.
(70) Zhou, J.; Schlegel, H. B. Ab initio classical trajectory study of the dissociation of neutral and positively charged methanimine (CH_2NH^n+ n = 0−2). *J. Phys. Chem. A* **2009**, *113*, 9958−9964.
(71) Mebel, A. M.; Bandrauk, A. D. Theoretical study of unimolecular decomposition of allene cations. *J. Chem. Phys.* **2008**, *129*, 224311.
(72) Xu, H.; Okino, T.; Yamanouchi, K. Ultrafast hydrogen migration in allene in intense laser fields: Evidence of two-body Coulomb explosion. *Chem. Phys. Lett.* **2009**, *469*, 255−260.
(73) Psciuk, B. T.; Tao, P.; Schlegel, H. B. Ab initio classical trajectory study of the fragmentation of C_3H_4 dications on the singlet and triplet surfaces. *J. Phys. Chem. A* **2010**, *114*, 7653−7660.
(74) Thachuk, M.; Wardlaw, D. M. Classical-analysis of diatomic dissociation dynamics in intense laser fields. *J. Chem. Phys.* **1995**, *102*, 7462−7471.
(75) Lee, S. K.; Li, W.; Schlegel, H. B. HCO+ dissociation in a strong laser field: An ab initio classical trajectory study. *Chem. Phys. Lett.* **2012**, *536*, 14−18.
(76) Shi, X. T.; Schlegel, H. B. Controlling the strong field fragmentation of $ClCHO^{+\cdot}$ using two laser pulses -an ab initio molecular dynamics simulation. *J. Comput. Chem.* **2019**, *40*, 200−205.
(77) Shi, X.; Thapa, B.; Li, W.; Schlegel, H. B. Controlling chemical reactions by short, intense mid-infrared laser pulses: Comparison of linear and circularly polarized light in simulations of $ClCHO^+$ fragmentation. *J. Phys. Chem. A* **2016**, *120*, 1120−1126.
(78) Lee, S. K.; Schlegel, H. B.; Li, W. Bond-selective dissociation of polyatomic cations in mid-infrared strong fields. *J. Phys. Chem. A* **2013**, *117*, 11202−11209.
(79) Thapa, B.; Schlegel, H. B. Molecular dynamics of methanol monocation (CH_3OH^+) in strong laser fields. *J. Phys. Chem. A* **2014**, *118*, 1769−1776.
(80) Thapa, B.; Schlegel, H. B. Molecular dynamics of methanol cation (CH_3OH^+) in strong fields: Comparison of 800 nm and 7 mu m laser fields. *Chem. Phys. Lett.* **2014**, *610*, 219−222.
(81) Thapa, B.; Schlegel, H. B. Molecular dynamics of methylamine, methanol, and methyl fluoride cations in intense 7 micron laser fields. *J. Phys. Chem. A* **2014**, *118*, 10067−10072.
(82) Tu, Y.-J.; Schlegel, H. B. Ab initio molecular dynamics study of the reactions of allene cation induced by intense 7 micron laser pulses. *Mol. Phys.* **2019**, *117*, 1088−1096.
(83) Krause, P.; Schlegel, H. B. Angle-dependent ionization of hydrides AH_n calculated by time-dependent configuration interaction with an absorbing potential. *J. Phys. Chem. A* **2015**, *119*, 10212−10220.
(84) Liao, Q.; Li, W.; Schlegel, H. B. Angle-dependent strong-field ionization of triple bonded systems calculated by time-dependent configuration interaction with an absorbing potential. *Can. J. Chem.* **2016**, *94*, 989−997.
(85) Winney, A. H.; Basnayake, G.; Debrah, D. A.; Lin, Y. F.; Lee, S. K.; Hoerner, P.; Liao, C.; Schlegel, H. B.; Li, W. Disentangling strong-field multielectron dynamics with angular streaking. *J. Phys. Chem. Lett.* **2018**, *9*, 2539−2545.
(86) Hoerner, P.; Schlegel, H. B. Angular dependence of strong field ionization of haloacetylenes HCCX (X = F, Cl, Br, I), using time-dependent configuration interaction with an absorbing potential. *J. Phys. Chem. C* **2018**, *122*, 13751−13757.
(87) Hoerner, P.; Li, W.; Schlegel, H. B. Angular dependence of strong field ionization of 2-phenylethyl-N,N-dimethylamine (PENNA) using time-dependent configuration interaction with an absorbing potential. *J. Phys. Chem. A* **2020**, *124*, 4777−4781.
(88) Pfeiffer, A. N.; Cirelli, C.; Smolarski, M.; Dorner, R.; Keller, U. Timing the release in sequential double ionization. *Nat. Phys.* **2011**, *7*, 428−433.
(89) Fleischer, A.; Worner, H. J.; Arissian, L.; Liu, L. R.; Meckel, M.; Rippert, A.; Dorner, R.; Villeneuve, D. M.; Corkum, P. B.; Staudte, A. Probing angular correlations in sequential double ionization. *Phys. Rev. Lett.* **2011**, *107*, 113003.
(90) Hoerner, P.; Li, W.; Schlegel, H. B. Sequential double ionization by strong laser fields simulated with time dependent configuration interaction. *J. Chem. Phys.* **2021**, *155*, 114103.
(91) Bamford, D. J.; Filseth, S. V.; Foltz, M. F.; Hepburn, J. W.; Moore, C. B. *J. Chem. Phys.* **1985**, *82*, 3032−3041.
(92) Debarre, D.; Lefebvre, M.; Péalat, M.; Taran, J.-P. E.; Bamford, D. J.; Moore, C. B. *J. Chem. Phys.* **1985**, *83*, 4476−4487.

https://doi.org/10.1021/acs.accounts.1c00390
Acc. Chem. Res. XXXX, XXX, XXX−XXX